Supplementary Materials

Aditya Tummala[1*], Francesca Marturano[2] and Giorgio Bonmassar[2]

[1*]Biomedical Engineering, Paulson School of Engineering and Applied Sciences, Harvard University, Boston, MA 02134, U.S.A.
[2]Department of Radiology, Athinoula A. Martinos Center for Biomedical Imaging, Harvard Medical School/Massachusetts General Hospital, Charlestown, MA 02129, U.S.A.

*Corresponding author(s). E-mail(s): adityatummala@college.harvard.edu;
Contributing authors: fmarturano@mgh.harvard.edu; giorgio.bonmassar@mgh.harvard.edu;

1 Complete Derivation

First, we simplify the particle emission source to a point at $S = (0, 0, 0)$. We center a cylindrical substrate W of radius R about the z-axis at $C = (0, D, 0)$, where D is defined as the distance between substrate center C and the emission source S, and take a cross-section in the x-y plane (Figure 1). We parametrize the bottom hemisphere of the circular cross–section of the cylinder by

$$P(\theta) = (R\cos\theta,\ R\sin\theta + D), \qquad \theta \in [\pi, 2\pi]. \tag{1}$$

as deposition only occurs on the bottom hemisphere of W facing the substrate. $\hat{n_p}(\theta)$ is the outward unit normal at deposition point P along the surface of the cross section and $\hat{n_{p0}}(\theta)$ is the same unit normal, but shifted to begin at S

$$\hat{n_{p0}}(\theta) = \hat{\boldsymbol{\imath}}\cos\theta + \hat{\boldsymbol{\jmath}}\sin\theta \tag{2}$$

where $\hat{\boldsymbol{\imath}}$ and $\hat{\boldsymbol{\jmath}}$ are versors in the x-axis and y-axis directions respectively and $\hat{n_p}(\theta) \parallel \hat{n_{p0}}(\theta)$. Let the particle emission source be simplified to a point at $S = (0, 0)$ (a

distance $D > 0$ below the center of the substrate cylinder) whereby the outward unit normal to the source is $\hat{n}_s = \hat{\boldsymbol{\jmath}}$. [1]
A ray of particles from the source S to the substrate at point P is therefore

$$\vec{r}(\theta) = \overrightarrow{SP(\theta)} = \hat{\boldsymbol{\imath}} R\cos\theta + \hat{\boldsymbol{\jmath}}(R\sin\theta + D), \qquad \theta \in [\pi, 2\pi] \tag{3}$$

with magnitude

$$\|\vec{r}(\theta)\| = \sqrt{R^2 + D^2 + 2RD\sin\theta} \tag{4}$$

and thus unit vector

$$\hat{r}(\theta) = \frac{\vec{r}(\theta)}{\|\vec{r}(\theta)\|} = \frac{\hat{\boldsymbol{\imath}} R\cos\theta + \hat{\boldsymbol{\jmath}}(R\sin\theta + D)}{\sqrt{R^2 + D^2 + 2RD\sin\theta}} \tag{5}$$

Then, the cosine of the emission angle $\psi(\theta)$ between $\hat{n_s}$ and $\hat{r}(\theta)$ can be defined as

$$\cos(\psi(\theta)) = \hat{r}(\theta)\cdot\hat{n}_s = \frac{(R\cos\theta)(0) + (R\sin\theta + D)(1)}{\|\vec{r}\|} = \frac{R\sin\theta + D}{\|\vec{r}\|} \tag{6}$$

and the incidence angle $\phi(\theta)$ between $\hat{n_p}$ and -$\hat{r}(\theta)$ can be defined as

$$\cos(\phi(\theta)) = -\hat{r}(\theta)\cdot\hat{n}_{p0} = \frac{(-R\cos\theta)(\cos\theta) + (-R\sin\theta - D)(\sin\theta)}{\|\vec{r}\|} = \frac{-R - D\sin\theta}{\|\vec{r}\|} \tag{7}$$

Since we seek to model a differential particle flux onto the differential area of deposition, we can use the property of solid angle to do so, as depicted in Figure **??**. Treating the differential deposition area as dA_p and the differential source area as dA_s, we have that the differential solid angle $d\omega$ $[sr]$, can be described as (Wang et. al. 2018)

$$d\omega = \frac{dA_p\cos(\phi(\theta))}{\|\vec{r}(\theta)\|^2} \tag{8}$$

Thus, in the cases when $\phi(\theta) = 0$, (by Figure 1, this occurs when $\theta = \frac{3\pi}{2}$), deposition is maximal, as $d\omega$ is at its maximum ($\cos(0) = 1 \Rightarrow d\omega = \frac{dA_p}{\|\vec{r}(\frac{3\pi}{2})\|^2}$).

1.1 Deposition Profile

With this geometric setup, we can describe $d\Phi_{emit}$ as the differential deposition rate at dA_p and $\mathcal{L}_s$ $[N_p s^{-1} m^{-2} sr^{-1}]$ as the particle radiance where N_p is defined as the number of particles. Then, as discussed in (Wang et. al. 2018), we have that

$$d\Phi_{emit}(\theta) = \mathcal{L}_s\cos^n(\psi(\theta))dA_s d\omega, \qquad [\Phi_{emit}] = [N_p s^{-1}] \tag{9}$$

Introducing equation Eq. (8) into Eq. (9), we attain

$$d\Phi_{emit}(\theta) = \mathcal{L}_s\frac{cos^n(\psi(\theta))\cos(\phi(\theta))}{\|\vec{r}(\theta)\|^2}dA_s dA_p \tag{10}$$

[1] Note: This geometric setup is defined so that film growth occurs in the negative $\hat{\jmath}$ direction, analogously to experimental PVD systems.

To determine the local particle deposition density $dJ_p(\theta)$ $[N_p m^{-2} s^{-1}]$, we divide by dA_p:

$$dJ_p(\theta) = \mathcal{L}_s \frac{cos^n(\psi(\theta))\cos(\phi(\theta))}{\|\vec{r}(\theta)\|^2} dA_s \tag{11}$$

Since we treat the source as a point emitter, integrating over its surface A_s gives us

$$J_p(\theta) = \int_{A_s} \mathcal{L}_s \frac{cos^n(\psi(\theta))\cos(\phi(\theta))}{\|\vec{r}(\theta)\|^2} dA_s \tag{12}$$

We collapse constants by defining constant $C = \mathcal{L}_s A_s$ $[N_p s^{-1}]$ and solve for $J_p(\theta)$:

$$J_p(\theta) = C \frac{cos^n(\psi(\theta))\cos(\phi(\theta))}{\|\vec{r}(\theta)\|^2} \tag{13}$$

Next, we define $P_s(\theta) \in [0, 1]$ as the sticking probability, i.e., the probability that a deposited particle adheres to those deposited before it. The rate of film growth $\dot{f}(t, \theta)$ $[ms^{-1}]$, then, is given by multiplying $J_p(\theta)$ by the particle volume $V_p[m^3 N_p^{-1}]$. Combining these factors, we define constant $K = CP_sV_p$ $[m^3 s^{-1}]$. Incorporating this into Eq. (13), we get

$$\dot{f}(t', \theta) = K \frac{cos^n(\psi(\theta))\cos(\phi(\theta))}{\|\vec{r}(\theta)\|^2} \tag{14}$$

Integrating over time, we calculate $f(t, \theta)$ $[m]$,

$$f(t, \theta) = \int_0^t \dot{f}(t', \theta) dt' = Kt \frac{cos^n(\psi(\theta))\cos(\phi(\theta))}{\|\vec{r}(\theta)\|^2} \tag{15}$$

Substituting Eq. (6) and Eq. (7) into Eq. (15),

$$f(t, \theta) = Kt \frac{(\frac{(D + R\sin\theta)}{\|\vec{r}(\theta)\|})^n (\frac{(-R - D\sin\theta)}{\|\vec{r}(\theta)\|})}{\|\vec{r}(\theta)\|^2}$$

$$f(t, \theta) = -Kt \frac{(D + R\sin\theta)^n (R + D\sin\theta)}{(R^2 + D^2 + 2RD\sin\theta)^{\frac{n+3}{2}}} \tag{16}$$

However, note that $\lim_{\theta \to \pi, 2\pi} f(t, \theta) < 0$. Specifically, this occurs where the term $R + D\sin(\theta) > 0$ (when $\sin(\theta) > -R/D$), i.e. near the boundaries approaching $\theta \to \pi, 2\pi$. In the raw analytic form, the model predicts small negative values near these edges because the cosine projection term allows for slight "overhang" where the surface normal begins to turn away from the source. However, in real physical vapor deposition, these regions simply receive negligible flux rather than negative deposition. Since we assume $D \gg R$, as is with almost all PVD systems, we can simplify the $R + D\sin(\theta)$ term to $D\sin(\theta)$, which is always negative across $\theta = \pi \to 2\pi$. Therefore, we attain a final equation, modeling deposition at any point $P(\theta)$ along

the circumference of the cylindrical substrate (fixed R) at time t:

$$\boxed{f(t,\theta) = -Kt\frac{(D + R\sin\theta)^n (D\sin\theta)}{(R^2 + D^2 + 2RD\sin\theta)^{\frac{n+3}{2}}}} \tag{17}$$

From above, we have that at some time t, substrate radius R, and angle around the substrate $\theta \in [\pi, 2\pi]$, the thickness of deposition at that point can be represented as Eq. (17). To evaluate the total conductive cross-section formed by the deposited material $A_{cs}(t)$ $[m^2]$, we integrate Eq. (17) over angle θ from $\pi \to 2\pi$ (cross section in the x-y plane):

$$A_{cs}(t) = \int_{\pi}^{2\pi} f(t,\theta) R d\theta, \qquad \theta \in [\pi, 2\pi] \tag{18}$$

For typical deposition conditions, the distance from the source to the substrate is significantly larger than the substrate radius ($R \ll D$). We therefore define the small parameter $\epsilon = \frac{R}{D} \ll 1$, and expand the above expression in powers of ϵ to isolate the leading-order dependence of the deposited cross-section on system geometry. Substituting Eq. (17) into Eq. (18), setting $R = \epsilon D$:

$$\begin{aligned}
A_{cs}(t) &= -Kt \int_{\pi}^{2\pi} \frac{D^n (1 + \epsilon\sin\theta)^n (D)(\sin\theta)}{(D^2(\epsilon^2 + 1 + 2\epsilon\sin(\theta))^{\frac{n+3}{2}}} R d\theta \\
&= -KtR \int_{\pi}^{2\pi} \frac{D^n (D)}{(D^2)^{\frac{n+3}{2}}} \frac{(\sin\theta)(1 + \epsilon\sin\theta)^n}{(\epsilon^2 + 1 + 2\epsilon\sin\theta)^{\frac{n+3}{2}}} d\theta \\
&= -KtR \frac{D^{n+1}}{D^{n+3}} \int_{\pi}^{2\pi} (\sin\theta) \frac{(1 + \epsilon\sin\theta)^n}{(\epsilon^2 + 1 + 2\epsilon\sin\theta)^{\frac{n+3}{2}}} d\theta \\
&= -\frac{KtR}{D^2} \int_{\pi}^{2\pi} (\sin\theta)(1 + \epsilon\sin\theta)^n (\epsilon^2 + 1 + 2\epsilon\sin\theta)^{-\frac{n+3}{2}} d\theta
\end{aligned} \tag{19}$$

Expanding to first order in $\epsilon = \frac{R}{D}$, dropping $O(\epsilon^2)$, by the binomial theorem, we have that $(1 + x)^a = 1 + ax + O(x^2) + O(x^3) + ...$ Applying this to Eq. (19), we expand each term in the integrand:

$$A_{cs}(t) = -\frac{KtR}{D^2} \int_{\pi}^{2\pi} (\sin\theta)(1 + n\epsilon\sin\theta + O(\epsilon^2))(-(\frac{n+3}{2})(2\epsilon\sin\theta) + 1 + O(\epsilon^2)) d\theta \tag{20}$$

Dropping second-order error terms ($O(\epsilon^2)$) at each step,

$$\begin{aligned}
A_{cs}(t) &\approx -\frac{KtR}{D^2} \int_{\pi}^{2\pi} (\sin\theta)(1 + n\epsilon\sin\theta)(1 - (n+3)\epsilon\sin\theta) d\theta \\
&\approx -\frac{KtR}{D^2} \int_{\pi}^{2\pi} (\sin\theta)(1 - (n\epsilon\sin\theta) - (3\epsilon\sin\theta) + (n\epsilon\sin\theta)) d\theta
\end{aligned}$$

$$\approx -\frac{KtR}{D^2}\int_{\pi}^{2\pi}(\sin\theta)(1-3\epsilon\sin\theta)d\theta$$
$$\approx -\frac{KtR}{D^2}\int_{\pi}^{2\pi}(\sin\theta-3\epsilon\sin^2\theta)d\theta$$
$$\approx -\frac{KtR}{D^2}(-2-3\epsilon(\frac{\pi}{2})). \tag{21}$$

Adding the error term $O(\epsilon^2)$ back in,

$$A_{cs}(t) \approx -\frac{KtR}{D^2}(-2-\frac{3\epsilon\pi}{2})+O(\epsilon^2) \tag{22}$$

Since $\epsilon = \frac{R}{D}$, substituting and distributing the **above expression (need to change to number**, we get our final expression for the cross-sectional area of deposition ($A_{cs}(t)$).

$$A_{cs}(t) \approx \frac{2KtR}{D^2}+\frac{3\pi KtR^2}{2D^3}+O(\frac{R^2}{D^2}), \qquad [A_{cs}(t)] = [m^2] \tag{23}$$

Here, the first term ($\frac{2KtR}{D^2}$) is dominant, the second term ($\frac{3\pi KtR^2}{2D^3}$) is a small correction ($\propto \frac{R}{D}$), and the rest is negligible by the aforementioned condition of $R \ll D$.

Now that we have the cross-sectional area of deposition A_{cs}, we can proceed with calculating the predicted resistance of the cylindrical substrate after time t seconds of deposition and a constant volumetric "flow-rate" of material K $[m^3 s^{-1}]$. First, we note that simple trace resistance is given by

$$\Omega = \frac{\rho L}{A} \tag{24}$$

where Ω $[\Omega = ohms]$ is resistance, ρ $[\Omega m]$ is the resistivity of deposited material, L $[m]$ is the length of the substrate, and A $[m^2]$ is the cross-sectional area of the substrate.

The resistivity ratio, using the correction for thin metal layers based on the Fuchs-Sondheimer (FS) and Mayadas-Shatzkes (MS) models (Jeong et al. (2023)) to account for boundary and scattering effects in thin films, is given by:

$$\frac{\rho_0}{\rho_{\text{eff}}} \simeq 1-\frac{3}{2}\alpha+3\alpha^2-3\alpha^3\log(1+\frac{1}{\alpha})-\frac{3(1-P)}{8k} \tag{25}$$

where ρ_{eff} $[\Omega m]$ depends on the thickness $f(t,\theta)$, ρ_0 $[\Omega m]$ is the bulk resistivity of Au, $k = \frac{f(t,\theta)}{l_0}$ $[mm^{-1}]$ (unitless), and P is the fraction of electrons specularly scattered at the external surfaces (Jeong et al. (2023); Mayadas (1968); Tellier and Tosser (1977)). Additionally, $\alpha = \frac{l_0 r_{gb}}{a_g(1-r_{gb})}$ $[\Omega m]$ whereby l_0 $[m]$ is the mean free path of electrons, r_{gb} $[m]$ is the grain boundary reflection constant, and a_g $[m]$ is average material crystalline diameter.

Let $F(\alpha) := 1 - \frac{3}{2}\alpha + 3\alpha^2 - 3\alpha^3 \log(1 + \frac{1}{\alpha})$. Then, by the FS-MS model, we have that

$$\frac{\rho_0}{\rho_{\text{eff}}} \cong F(\alpha) - \frac{3(1-P)}{8k} = F(\alpha) - \frac{3(1-P)}{8}\frac{l_0}{f(t,\theta)} \tag{26}$$

To calculate the resistance across the entire cylindrical substrate, we can find longitudinal conductance per unit length $G(t)$ as the parallel sum over the cross-section of the cylindrical substrate

$$G(t) = \int_{\pi}^{2\pi} \sigma_{eff}(f(t,\theta))f(t,\theta)Rd\theta, \tag{27}$$

where effective conductance $\sigma_{eff}(f(t,\theta)) = (\rho_{eff}(f(t,\theta)))^{-1}$. Thus substituting into Eq. (26),

$$\begin{aligned}
\rho_0\sigma_{eff}(f(t,\theta)) &\simeq F(\alpha) - \frac{3-3P}{8}\frac{l_o}{f(t,\theta)} \\
\sigma_{eff}(f(t,\theta)) &\simeq \frac{F(\alpha)}{\rho_0} - \frac{3-3P}{8}\frac{l_o}{\rho_0 f(t,\theta)}
\end{aligned} \tag{28}$$

Substituting Eq. (28) into Eq. (27) to find $G(t)$,

$$\begin{aligned}
G(t) &= \int_{\pi}^{2\pi} [\frac{F(\alpha)}{\rho_0} - \frac{3-3P}{8}\frac{l_o}{\rho_0 f(t,\theta)}]f(t,\theta)Rd\theta \\
&= \frac{F(\alpha)}{\rho_0}\int_{\pi}^{2\pi} \underbrace{f(t,\theta)Rd\theta}_{A_{cs}} - \int_{\pi}^{2\pi} \frac{3-3P}{8}\frac{l_o}{\rho_0}Rd\theta \\
&= \frac{F(\alpha)}{\rho_0}A_{cs}(t) - \frac{3-3P}{8}\frac{l_o}{\rho_0}\int_{\pi}^{2\pi} Rd\theta \\
&= \frac{F(\alpha)}{\rho_0}A_{cs}(t) - \frac{3-3P}{8}\frac{l_o}{\rho_0}\pi R \\
&= \frac{1}{\rho_0}[F(\alpha)A_{cs}(t) - \frac{3-3P}{8}\pi R l_0]
\end{aligned} \tag{29}$$

Therefore, since resistance $R_{cyl} = G(t)^{-1}$,

$$\begin{aligned}
R_{cyl}(t) &\cong \frac{L_{cyl}\rho_0}{F(\alpha)A_{cs}(t) - \frac{3-3P}{8}\pi R l_0} \\
&= \frac{L_{cyl}\rho_0}{F(\alpha)(\frac{2KtR}{D^2} + \frac{3\pi KtR^2}{2D^3} + O(\frac{R^3}{D^4})) - \frac{3-3P}{8}\pi R l_0} \\
&= \frac{L_{cyl}\rho_0}{F(\alpha)(\frac{2KtR}{D^2})(1 + \frac{3\pi R}{4D} + O(\frac{R^2}{D^2})) - \frac{3-3P}{8}\pi R l_0}
\end{aligned} \tag{30}$$

To account for ambient deposition temperatures $T_{amb} \neq 25°C$, in addition to modifications to the temperature-dependent constants listed above, we adjust R_{cyl} by temperature-dependent constant $T_{adj} := (1 + \alpha(T_{amb} - 25°C))$(Jeong et. al. 2023):

$$= \frac{L_{cyl}\rho_0}{F(\alpha)(\frac{2KtR}{D^2})(1 + \frac{3\pi R}{4D} + O(\frac{R^2}{D^2})) - \frac{3-3P}{8}\pi R l_0} T_{adj} \tag{31}$$

Simplifying further,

$$\boxed{R_{cyl}(t) = \frac{L_{cyl}\rho_0 T_{adj}}{R[F(\alpha)(\frac{2Kt}{D^2})(1 + \frac{3\pi R}{4D} + O(\frac{R^2}{D^2})) - \frac{3-3P}{8}\pi l_0]}, \qquad R \ll D} \tag{32}$$

where $F(\alpha) = 1 - \frac{3}{2}(\frac{l_0 r_{gb}}{a_g(1-r_{gb})}) + 3(\frac{l_0 r_{gb}}{a_g(1-r_{gb})})^2 - 3(\frac{l_0 r_{gb}}{a_g(1-r_{gb})})^3 \log(1 + \frac{a_g(1-r_{gb})}{l_0 r_{gb}})$ and $T_{adj} = (1 + \frac{l_0 r_{gb}}{a_g(1-r_{gb})}(T_{amb} - 25°C))$.

2 Additional Characterization

As discussed in Section 5.2.3 of the main article, we see island formation, flaking, and cracking on wire substrates post-deposition (See Supplementary Figure 1).

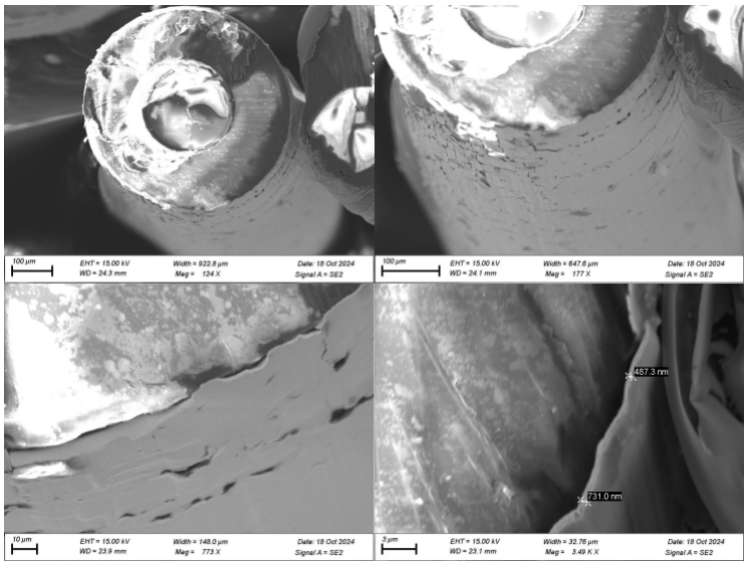

Fig. 1 SEM images of wire substrate cross section after 1 μm Au deposition, noting the island formation and flaking of the trace.

3 Project Resources

All code developed for this study is open-access, and is available on GitHub.

References

Jeong H, Ntolkeras G, Warbrick T, et al (2023) Aluminum thin film nanostructure traces in pediatric eeg net for mri and ct artifact reduction. Sensors 23(7). https://doi.org/10.3390/s23073633

Mayadas AF (1968) Intrinsic resistivity and electron mean free path in aluminum films. Journal of Applied Physics 39(9):4241–4245. https://doi.org/10.1063/1.1656954

Tellier CR, Tosser AJ (1977) Size effects in thin films. Thin Solid Films 41(1):1–20. https://doi.org/10.1016/0040-6090(77)90309-1